

Myeloid cell-specific *Irf5* deficiency stabilizes atherosclerotic plaques in *Apoe*^{-/-} mice



Julia Leipner¹, Tsai-Sang Dederichs¹, Alexander von Ehr¹, Simon Rauterberg¹, Carolin Ehlert¹, Julian Merz¹, Bianca Dufner¹, Natalie Hoppe¹, Katja Krebs¹, Timo Heidt¹, Constantin von zur Muehlen¹, Peter Stachon¹, Klaus Ley², Dennis Wolf¹, Andreas Zirlik³, Christoph Bode¹, Ingo Hilgendorf^{1,*,*,4}, Carmen Härdtner^{1,*,4}

ABSTRACT

Objective: Interferon regulatory factor (IRF) 5 is a transcription factor known for promoting M1 type macrophage polarization *in vitro*. Given the central role of inflammatory macrophages in promoting atherosclerotic plaque progression, we hypothesize that myeloid cell-specific deletion of *IRF5* is protective against atherosclerosis.

Methods: Female *Apoe*^{-/-} *Lysm*^{Cre/+} *Irf5*^{fl/fl} and *Apoe*^{-/-} *Irf5*^{fl/fl} mice were fed a high-cholesterol diet for three months. Atherosclerotic plaque size and compositions as well as inflammatory gene expression were analyzed. Mechanistically, IRF5-dependent bone marrow-derived macrophage cytokine profiles were tested under M1 and M2 polarizing conditions. Mixed bone marrow chimeras were generated to determine intrinsic IRF5-dependent effects on macrophage accumulation in atherosclerotic plaques.

Results: Myeloid cell-specific *Irf5* deficiency blunted LPS/IFN γ -induced inflammatory gene expression *in vitro* and in the atherosclerotic aorta *in vivo*. While atherosclerotic lesion size was not reduced in myeloid cell-specific *Irf5*-deficient *Apoe*^{-/-} mice, plaque composition was favorably altered, resembling a stable plaque phenotype with reduced macrophage and lipid contents, reduced inflammatory gene expression and increased collagen deposition alongside elevated *Mertk* and *Tgfb3* expression. *Irf5*-deficient macrophages, when directly competing with wild type macrophages in the same mouse, were less prone to accumulate in atherosclerotic lesion, independent of monocyte recruitment. *Irf5*-deficient monocytes, when exposed to oxidized low density lipoprotein, were less likely to differentiate into macrophage foam cells, and *Irf5*-deficient macrophages proliferated less in the plaque.

Conclusion: Our study provides genetic evidence that selectively altering macrophage polarization induces a stable plaque phenotype in mice.

© 2021 The Authors. Published by Elsevier GmbH. This is an open access article under the CC BY-NC-ND license (<http://creativecommons.org/licenses/by-nc-nd/4.0/>).

Keywords Atherosclerosis; Interferon regulatory factor 5; Macrophage polarization (M1, M2); Plaque stabilization; Anti-inflammation; Aortic macrophages

1. INTRODUCTION

Cardiovascular (CV) disease is the leading cause of morbidity and mortality. Despite optimal secondary prevention, CV deaths account for almost one third of all deaths worldwide [1]. Atherosclerosis is the underlying pathomechanism in most

cases, considered a chronic, lipid-driven inflammatory disease [2–6].

In the developing plaque, monocytes infiltrate the arterial intima and differentiate into macrophages which proliferate locally, driven by oxidized low density lipoprotein (LDL) uptake [3,4,6]. Macrophages in the plaque are thought to preserve plasticity, changing their phenotype

¹University Heart Center, Department of Cardiology and Angiology I, University of Freiburg and Faculty of Medicine, 55 Hugstetter St, 79106, Freiburg, Germany ²La Jolla Institute for Allergy & Immunology, Division of Inflammation Biology, 9420 Athena Circle, La Jolla, CA, 92037, USA ³LKH-University Hospital Graz, Department of Cardiology, Auenbruggerplatz 15, 8036, Graz, Austria

⁴ Ingo Hilgendorf and Carmen Härdtner contributed equally to this work.

*Corresponding author.

**Corresponding author. Immunocardiology, Breisacher street 33, 79106, Freiburg i.Br., Germany.

E-mails: julia.leipner@universitaets-herzzentrum.de (J. Leipner), tsai-sang.dederichs@uniklinik-freiburg.de (T.-S. Dederichs), alexander.von.ehr@uniklinik-freiburg.de (A. von Ehr), simon.rauterberg@uniklinik-freiburg.de (S. Rauterberg), carolin.ehlert@universitaets-herzzentrum.de (C. Ehlert), julian.merz@universitaets-herzzentrum.de (J. Merz), bianca.dufner@universitaets-herzzentrum.de (B. Dufner), natalie.hoppe@universitaets-herzzentrum.de (N. Hoppe), katja.krebs@uniklinik-freiburg.de (K. Krebs), timo.heidt@universitaets-herzzentrum.de (T. Heidt), constantin.vonzurmuehlen@universitaets-herzzentrum.de (C. von zur Muehlen), peter.stachon@universitaets-herzzentrum.de (P. Stachon), klaus@lilai.org (K. Ley), dennis.wolf@universitaets-herzzentrum.de (D. Wolf), andreas.zirlik@medunigraz.at (A. Zirlik), christoph.bode@universitaets-herzzentrum.de (C. Bode), ingo.hilgendorf@universitaets-herzzentrum.de (I. Hilgendorf), carmen.haerdtnern@universitaets-herzzentrum.de (C. Härdtner).

Abbreviations: IRF5, Interferon regulatory factor 5; LYVE1, Lymphatic Vessel Endothelial Hyaluronidase; NEAA, Non-essential amino acids; MRC1, Mannose Receptor C-Type 1

Received February 23, 2021 • Revision received May 6, 2021 • Accepted May 7, 2021 • Available online 12 May 2021

<https://doi.org/10.1016/j.molmet.2021.101250>

according to the cytokine composition in the environment [7]. Single-cell analyses have recently identified several populations of macrophages in the atherosclerotic aorta, most prominently a population of resident-like macrophages, “foamy”, lipid-rich macrophages expressing high levels of Triggering receptor expressed on myeloid cells (*Trem*) 2, and inflammatory macrophages [5,8]. Although macrophage heterogeneity in the plaque appears more complex than the traditional M1 and M2 type polarization states, the dichotomous concept of inflammation driving and resolving macrophage subsets prevails [9–11].

Interferon regulatory factor (IRF) family members are transcription factors, which are involved in the regulation of immune cell development, differentiation, and responses to pathogens. IRF3, 5, 7, and 8 mediate the response to viral RNA and DNA downstream of pathogen recognition receptors [12]. IRF4, 5, and 8 regulate myeloid cell development and phenotype [12]. IRF5 is predominantly expressed in B cells, monocytes, macrophages, and plasmacytoid dendritic cells (pDCs) [13,14]. However, IRF5 expression has also been reported in classic DCs, T-cells, fibroblasts, endothelial cells (ECs) and adipocytes, and thus in a plethora of atheroma-associated cell types [15–20]. In macrophages, for example, IRF5 acts downstream of Myd88-associated Toll-like receptors (TLR) inducing expression of pro-inflammatory cytokines such as Interleukin (IL)-6, IL-12, Tumor Necrosis Factor (TNF)- α , Interferon gamma (IFN- γ) and IL-23, and repressing the expression of anti-inflammatory IL-10 and transforming growth factor (TGF) β [15,20–25]. Therefore, transcription factor IRF5 is best known for mediating M1 polarization in macrophages, whereas IRF4 triggers M2 polarization while competing for the same binding sites at Myd88 [12,15,24,26,27]. In the plaque environment, high mobility group box 1 (HMGB1), heat shock protein (HSP)60, modified LDL and nucleic acid polymers activate Myd88-dependent TLR pathways upstream of IRF5 [28–30].

In this study, we show that selective *Irf5* deficiency in macrophages is sufficient to generate a stable plaque phenotype in mice, providing a rationale for modulating macrophage phenotypes in order to combat atherosclerosis.

2. MATERIALS AND METHODS

2.1. Animals and diet

Wild type (WT) CD45.1⁺ (B6 CD45.1), *Apoe*^{-/-}, *Apoe*^{-/-} *Irf5*^{fl/fl} and *Apoe*^{-/-} *Lysm*^{Cre/+} *Irf5*^{fl/fl} were housed under specific pathogen-free conditions. Myeloid cell-specific *Irf5*^{-/-} (*Apoe*^{-/-} *Lysm*^{Cre/+} *Irf5*^{fl/fl}) and *Irf5*^{+/+} mice (*Apoe*^{-/-} *Irf5*^{fl/fl}) were generated through cross-breeding of *Apoe*^{-/-} (B6.129P2-*Apoe*^{tm1Unc/J}), *Lysm*^{Cre/Cre} (B1.129P2-*Lyz2*^{tm1(Cre)flto/J}) and *Irf5*^{fl/fl} (C57BL/6-*Irf5*^{tm1Ppr/J}) mice (kindly provided by Klaus Ley, San Diego, CA, USA) (Figure 2A). Eight to 10-week-old female *Apoe*^{-/-} *Irf5*^{fl/fl} and *Apoe*^{-/-} *Lysm*^{Cre/+} *Irf5*^{fl/fl} mice were fed a high-cholesterol diet (HCD, 1.25% w/w cholesterol, D12108 mod., Sniff GmbH, Soest, Germany) ad libitum for 12 weeks to accelerate atherosclerotic plaque formation. Male *Apoe*^{-/-} mice develop cutaneous ulcerations more frequently under HCD for which reason the Animal Care Committee of the University of Freiburg and the Regional Council, who approved all protocols, advised against the use of male mice in this study.

To generate mixed chimeras, 8 week-old female *Apoe*^{-/-} mice were lethally irradiated 9.5 Gy, irradiator IBL637C γ -ray ¹³⁷Cs (Schering Cis-Bio International, France) and reconstituted with 6×10^6 bone marrow cells from WT CD45.1⁺ *Apoe*^{-/-} and CD45.2⁺ *Apoe*^{-/-} *Lysm*^{Cre/+} *Irf5*^{fl/fl} donor animals. Donor cells were mixed 1:1 and injected into the recipient *Apoe*^{-/-} animals intravenously. Six weeks post bone marrow

transplantation, the reconstituted mixed chimeric mice were fed a HCD for 12 weeks to accelerate atherogenesis.

2.2. Histology

Murine aortic roots were embedded in OCT Tissue Tek (Sakura Finetek, Tokyo, Japan) and cut into serial cryostat sections (5 μ m) starting at the level of the aortic valve. Aortic arches were sectioned longitudinally, and plaques were analyzed along a 2 mm section of the lesser curvature. Sections were stained with Oil-red O (Sigma Aldrich, St. Louis, MO, USA), Masson Trichrome (Sigma Aldrich, St. Louis, MO, USA), anti-CD68 (clone FA-11, BioRad AbD Serotec, Purchheim, Germany), secondary antibodies rabbit-anti rat biotin conjugated (BA-4001) according to the manufacturers' instructions (see [3]). Images were recorded with the Axioplan 2 imaging light-/fluorescence microscope (Carl Zeiss MicroImaging GmbH, Göttingen, Germany). Images were analyzed with Image Pro Premiere 9.2 (Media Cybernetics, Silver Springs, USA).

2.3. Flow cytometry

Murine aortic cells were retrieved through enzymatic digestion with collagenase I, collagenase XI, hyaluronidase, DNase I and HEPES Solution (Sigma Aldrich, St. Louis, MO, USA) in a thermocycler for 45 min at 750 rpm and 37 °C. Murine blood samples were lysed in red blood cell lysis buffer (Biolegend, San Diego, CA, USA). Isolated cells from the blood and aorta were counted using a Neubauer Chamber (Marienfeld, Lauda-Königshofen, Germany).

Cells were stained with specific fluorescent antibodies as indicated in supplemental table 1. Bone marrow-derived macrophages (BMDMs) were stained with a viability dye (Fixable Viability Dye, eFlour450, eBioscience, Thermo Fisher Scientific, Waltham, MA, USA), according to the manufacturer's protocol, prior to adding fluorescent antibodies. Ly6C^{high} monocytes were identified as CD45⁺, CD11b⁺, Lin⁻ (Lin = CD3, CD19, NK1.1, Ly6G), Ly6C^{high}, CD115⁺, F4/80^{low}. Macrophages were identified as CD45⁺, CD11b⁺, Lin⁻, Ly6C^{low}, F4/80^{high}. Neutrophils were identified as CD45⁺, CD11b⁺, Ly6G⁺. T-cells as CD45⁺, CD11b⁻, CD3⁺, CD19⁻ and B-cells as CD45⁺, CD11b⁻, CD19⁺, CD3⁻. Intracellular staining with anti-Ki67 and anti-active Caspase 3, BD Cytofix/Cytoperm (#554722, BD Biosciences, San Diego, CA, USA), BD Perm/Wash (#554723) and BD Permeabilization Buffer Plus (#561651) was conducted according to the manufacturer's instructions. Data were collected on a BD FACSCanto II Cell Analyzer (BD Bioscience, San Diego, CA, USA) and analyzed with FlowJo (Treestar, Ashland, OR, USA). Aortic macrophages were sorted into RLT-buffer/1% β -mercaptoethanol (Sigma Aldrich, St. Louis, MO, USA), (RLT-buffer out of RNeasy Micro Kit (Qiagen, Valencia, CA, USA)) by a BD FACSAria Fusion Cell Sorter (BD Bioscience, San Diego, CA, USA). Monocytes from blood and spleen were sorted in (Roswell Park Memorial Institute (RPMI)-1640, 10% fetal calf serum (FCS), 1% non-essential amino acids (NEAA), 1% Penicillin/Streptomycin (PenStrep)) for further cultivation.

2.4. Real-time qPCR

RNA was extracted from murine whole aortas using QIAzol and RNeasy Mini Kit (Qiagen, Valencia, CA, USA) or BMDMs using RNeasy Mini Kit or from sorted aortic macrophages using QIAshredder and RNeasy Micro Kit (Qiagen, Valencia, CA, USA) according to the manufacturer's instructions. Quantitative TaqMan-PCR was performed using a Bio-Rad CFX96 Touch Real-Time PCR System and TaqMan probes Mm00443258_m1 (*Tnfrsf*), Mm01336189_m1 (*Pro11b*), Mm00439614_m1 (*Irf10*), Mm01178820_m1 (*Tgfb1*), Mm00441242_m1 (*Ccl2*), Mm00496478_g1 (*Irf5*), Mm01320970_m1 (*Vcam-1*), Mm00434920_m1 (*Mertk*), Mm0048

5148_m1 (*Mrc1*), Mm00475988_m1 (*Arg1*), Mm00439498_m1 (*Mmp2*), Mm00516023_m1 (*Icam-1*), Mm01302427_m1 (*Ccl5*), Mm00434174_m1 (*Ii12*), Mm01135198_m1 (*Cd36*), Mm00442646_m1 (*Abca1*) (Thermo Fisher Scientific, Waltham, MA, USA). Data were statistically analyzed using the $2^{-\Delta\Delta Ct}$ method.

2.5. BMDMs

Bone marrow cells were isolated from myeloid cell-specific *Irf5*^{-/-} (*Apoe*^{-/-} *Lysm*^{Cre/+} *Irf5*^{fl/fl}) and WT (*Apoe*^{-/-} *Irf5*^{fl/fl}) mice. Cells were stimulated with 30 ng/mL macrophage colony-stimulating factor (M-CSF) (PeproTech, Rocky Hill, NJ, USA) in normal culture media (RPMI-1640, 10% FCS, 1% NEAA, 1% PenStrep) and differentiated into macrophages for 5–7 days. Unstimulated M0 macrophages were polarized to either M1 or M2 macrophages by co-incubation with 100 ng/mL lipopolysaccharide (LPS) and 10 ng/mL Interferon gamma (IFN), or 20 ng/mL IL-4 and 20 ng/mL IL-13 (PeproTech, Rocky Hill, NJ, USA) in RPMI-1640/0.1% FCS/1% NEAA for 12 h, respectively.

2.6. Monocyte to macrophage differentiation and oxidized (ox)LDL uptake

Monocytes were sorted from blood and spleen cell suspensions and cultivated in RPMI-1640, 10% FCS, 1% NEAA, 1% PenStrep with 30 ng/mL M-CSF overnight (16 h) for differentiation into F4/80^{high} macrophages. During the final 4 h of macrophage differentiation, cells were incubated with 10 µg/mL human Dil-labeled medium oxidized LDL (Dil-oxLDL, Kalen Biomedical, Montgomery Village, MD, USA). Foam cell formation and differentiation was evaluated by flow cytometry (defined as Viability Dye⁻ F4/80^{high} Dil⁺ macrophages).

2.7. Cholesterol assays

Murine plasma cholesterol levels were measured using Cholesterol FS 10' Multi-purpose kit (DiaSys Diagnostic Systems GmbH, Holzheim, Germany) according to the manufacturer's instructions.

2.8. Bioinformatic integration of single-cell datasets and visualization of IRF5 expression

The expression matrix table and sample information were downloaded from Gene Expression Omnibus dataset GSE131776 [31] and generously provided by Dr. Dennis Wolf [32]. We only retained the TCF21 WT samples from Wirka et al. for the analysis. We used the R package Seurat (version 3.2) [33,34] to integrate the *Apoe*^{-/-} mouse dataset from both publications. We first performed the standard Seurat workflow on each dataset separately. Briefly, after log-normalization with the scale factor of 10,000, the 2000 most variable genes selected with variance stabilizing transformation were used for principle component analysis. We applied the function RunTSNE to use the first 20 principle components for dimensionality reduction. Graph-based clustering was performed by FindNeighbors and FindClusters with a resolution of 0.65 and 1.2 for the Wirka et al. and Winkels et al. datasets, respectively. Cell types were assigned to clusters according to the signatures suggested in the original publications. The expression matrix and metadata with cell type information of both datasets were combined and used for another standard Seurat analysis. The parameters were kept the same except that the resolution was set at 0.8 for clustering. The two datasets were well integrated with macrophage and T cell clusters from each dataset overlapping. For the simplicity of presentation, we annotated the subclusters of smooth muscle cells and T cells as larger clusters. Sub-analysis of macrophages was performed by

extracting the macrophage subset from the Seurat object and running another Seurat analysis with the same parameters as mentioned above. We annotated the sub-groups of macrophage according to the known macrophage subset markers — inflammatory (*Tnf* and *Ii1b*), resident-like (Mannose Receptor C-Type1 (*Mrc1*) and Lymphatic Vessel Endothelial Hyaluronan Receptor 1 (*Lyve1*)), and foamy (Triggering Receptor Expressed On Myeloid Cells 2 (*Trem2*) and ATP Binding Cassette Subfamily G Member 1 (*Abcg1*)) [8]. We applied the macrophage matrix and metadata with macrophage subset information for Seurat v3 integration. We used the functions, FindIntegrationAnchors and IntegrateData, as recommended by Seurat guidelines [35]. The same Seurat analysis procedure was performed on the human right coronary artery dataset. Cell type annotation was assigned according to the original publication. Analysis and annotation of macrophage subset were performed with the same settings and features that applied for mouse macrophage data analysis. The human dataset composed of samples from four patients was fairly well integrated but not as uniformly as the mouse dataset, likely due to the differences of cell composition and cell counts from each individual as well as larger variation between humans. Hence, we performed Seurat v3 integration for all cell types and macrophages from human with the same settings that were applied to mouse macrophage dataset. Expression of features and *IRF5* was visualized by the Seurat tools, Featureplot and Vlnplot.

2.9. Statistics

Results are presented as mean + standard error of the mean (SEM). Differences between two groups from independent mice or samples were analyzed with the unpaired Student's t test (if $n > 5$ and passing D'Agostino and Pearson omnibus normality test) or with Mann–Whitney test (if $n \leq 5$ or not normally distributed). To assess differences between more than 2 groups Kruskal Wallis (if $n \leq 5$ or not normally distributed) and a subsequent Dunn's multiple comparisons test was applied. P values ≤ 0.05 denote significant changes. Gene expression comparison between subtypes of macrophages were performed with the Seurat tool, FindMarkers, using a Wilcoxon Rank–Sum test.

3. RESULTS

3.1. Macrophages are the dominant IRF5-expressing cell type in atherosclerotic lesions

Irf5 expression was reported in monocytes, macrophages, DCs, B- and T-cells, fibroblasts and endothelial cells [13–20] — cells that can be found in atherosclerotic lesions. To evaluate *Irf5* expression in atheroma-associated cells directly, we inquired single-cell gene expression profiles from atherosclerotic aortic lesions in *Apoe*^{-/-} mice [31,32]. While a minority of fibroblasts and vascular smooth muscle cells expressed *Irf5*, a large proportion of B cells, monocytes and macrophages, in particular, expressed *Irf5* (Figure 1A). *Irf5* expression increased in the population of aortic macrophages during HCD-induced atherosclerosis formation in *Apoe*^{-/-} mice (Supplemental Fig. 1A). Single-cell analysis and subclustering of macrophages into inflammatory, resident-like, and foamy subsets showed that *Irf5* expression was wide-spread and not significantly enriched in a specific macrophage subtype in mice (Figure 1B and Supplemental Fig. 1B). Notably, single-cell RNAseq analysis of human plaques identified a similar *IRF5* expression pattern in- and outside macrophages, and *IRF5* expression being highest in foamy and inflammatory macrophages (Figure 1C, D Supplemental Fig. 1D).

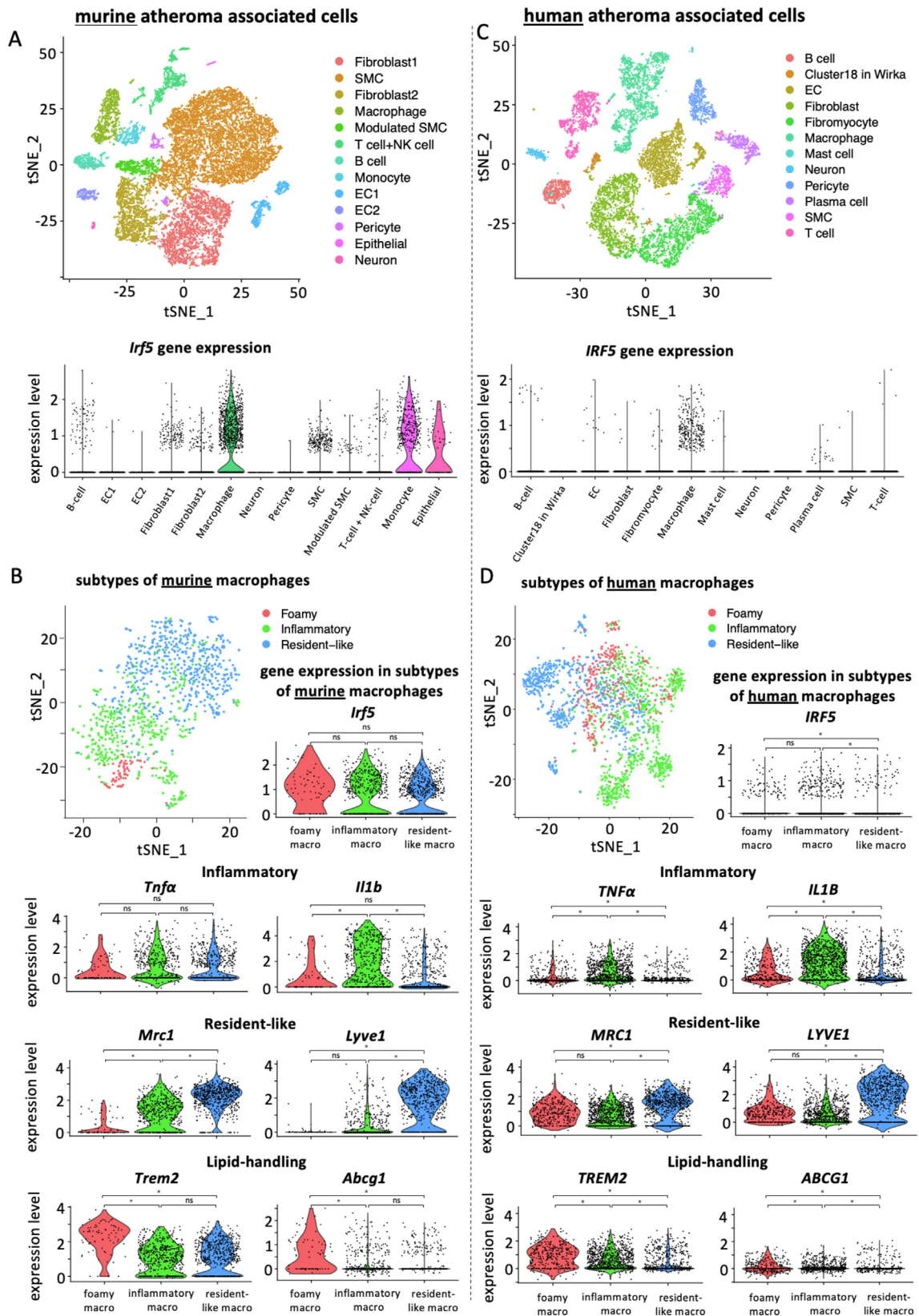


Figure 1: scRNA-Seq datasets from murine (Winkels et al., 2018 + Wirka et al., 2019, data integrated) and human (Wirka et al., 2019) atherosclerotic lesions were analyzed for *Irf5* expression. (A, C) tSNE plots of mouse and human atheroma associated cell types and *Irf5* expression herein (violin plots). (B, D) tSNE plots depicting foamy, inflammatory, and resident-like subtypes of murine (Winkels et al., 2018 + Wirka et al., 2019, data integrated) and human macrophages (Wirka et al., 2019) in atherosclerotic lesions. Violin plots showing expression levels of *Irf5* and subtype defining genes in the respective macrophage subtypes. * $p < 0.05$ denotes statistically significant differences between macrophage subsets, adjusted p-value, Wilcoxon Rank-Sum test.

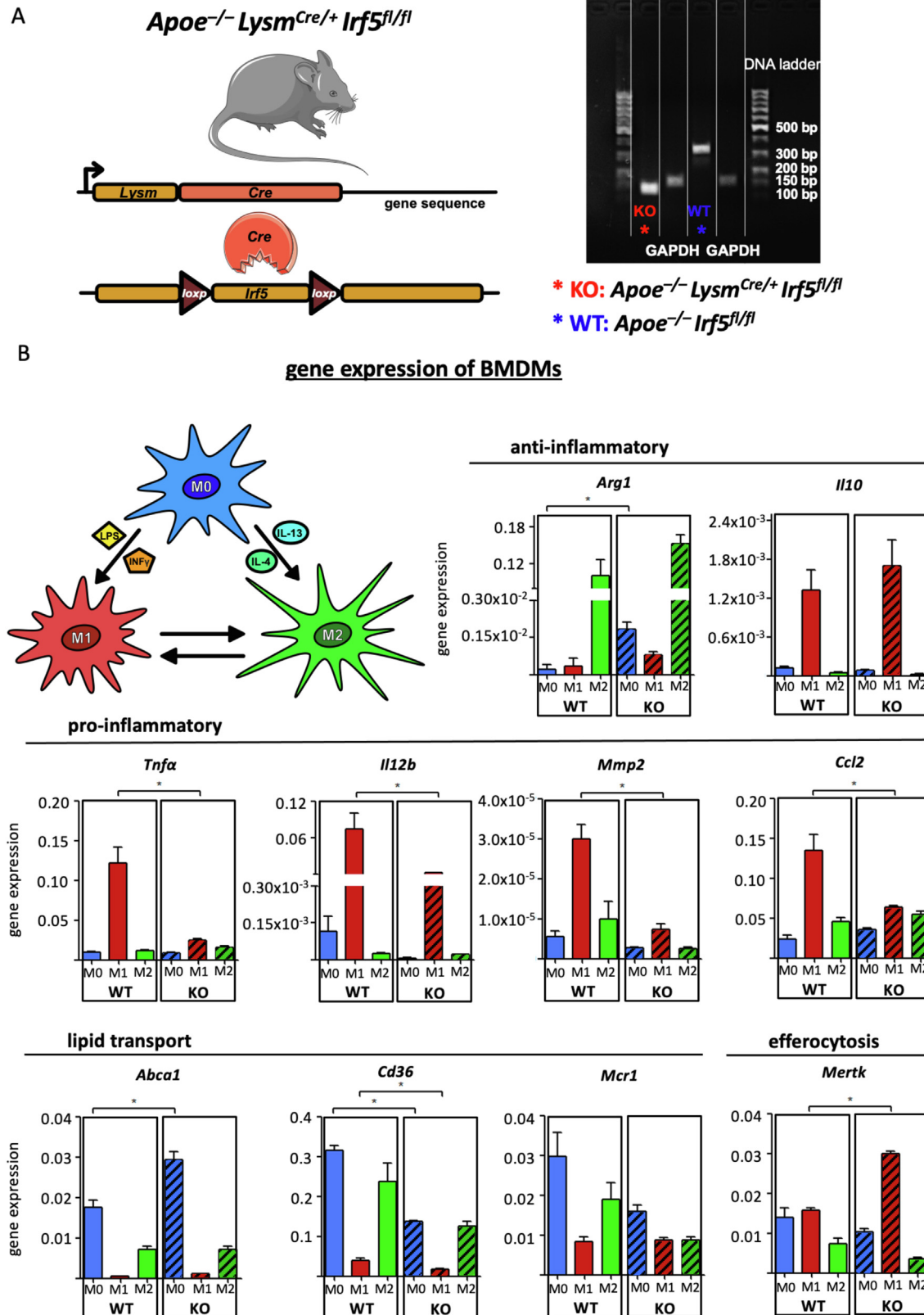


Figure 2: (A) Confirmation of myeloid cell-specific *Irf5* deficiency in Bone-marrow derived macrophages (BMDM) isolated from *Apoe*^{-/-} *Lysm*^{Cre/+} *Irf5*^{fl/fl} mice (KO) and WT controls (*Apoe*^{-/-} *Irf5*^{fl/fl} mice) by gel-electrophoresis of *Irf5* PCR products. (B) BMDM generated from WT and KO bone marrow cells (M0) were polarized to M1 and M2 subsets *in vitro* through stimulation with LPS and IFN γ or IL-4 and IL-13 for 12 h. Results of expressions for key macrophage-associated genes are presented as mean \pm SEM. Gene expressions were analyzed using the $\Delta\Delta C_q$ method and normalized to the expression of β -actin. * $p < 0.05$ denotes statistically significant differences between macrophage subtypes, Mann–Whitney, $n = 4$ per group. IFN γ = interferon, IL = interleukin, LPS = lipopolysaccharide, WT = wild type.

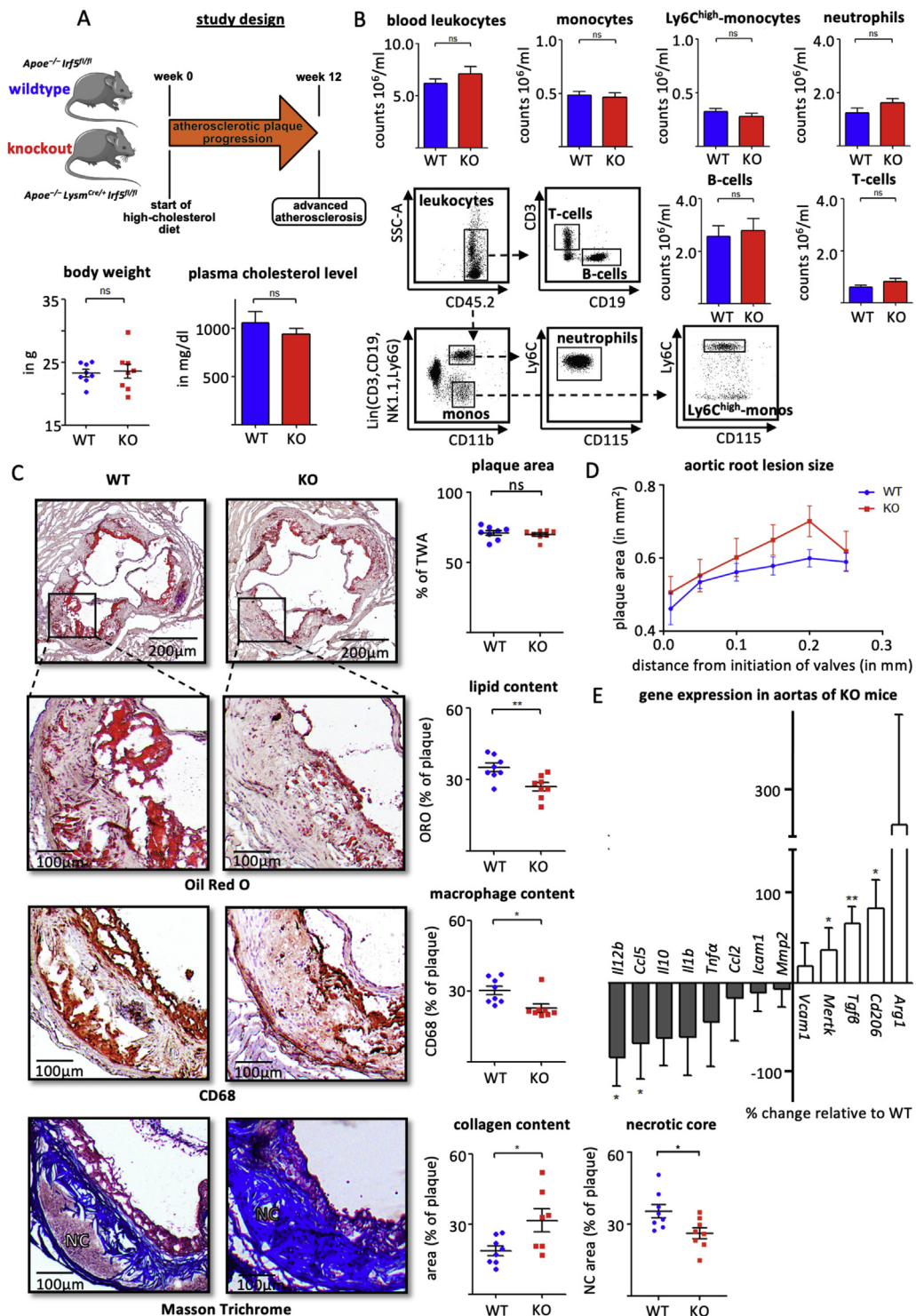


Figure 3: (A) Myeloid cell-specific *Irf5* deficient *Apoe^{-/-}* mice (KO) and WT controls were fed a high cholesterol diet for 12 weeks. Body weight and plasma cholesterol levels are presented as mean \pm SEM, n = 8 per group. ns = non-significant, t-test. (B) Representative dot plots and cell counts for leukocytes, neutrophils, monocytes, Ly6C^{high}-monocytes in particular, T-cells and B-cells in the blood are presented as mean \pm SEM, n = 8 per group. ns = non-significant, t-test. (C) Representative histologic images and quantification of plaque area, lipid- (Oil Red O), macrophage- (CD68), collagen-contents and necrotic core (Masson Trichrome), and necrotic core (NC) in aortic root sections. The plaque area represents the intimal lesion area as a fraction of the total wall area (encompassing intima and media). Areas within lesions filled with lipids, macrophages, collagen and the necrotic core are related to the intimal lesion area. Results are presented as mean percentage \pm SEM, n = 8 per group. *p < 0.05 denotes statistically significant differences between WT and KO mice, t-test. (D) Absolute aortic root lesion size measured in 6 serial sections at 50 μ m intervals starting from valve initiation. Results are presented as mean \pm SEM, n = 8 per group. ns = non-significant, t-test. (E) Change in gene expressions in aortas from myeloid cell-specific *Irf5* KO-mice relative to expression levels in WT mice. Gene expressions were analyzed using the $\Delta\Delta$ Cq method and normalized to the expression of β -actin. Results are presented as mean \pm SEM, n = 8 per group. *p < 0.05 denotes statistically significant differences between WT and KO, t-test and Mann–Whitney. ORO=Oil red O, TWA = total wall area, NC = necrotic core.

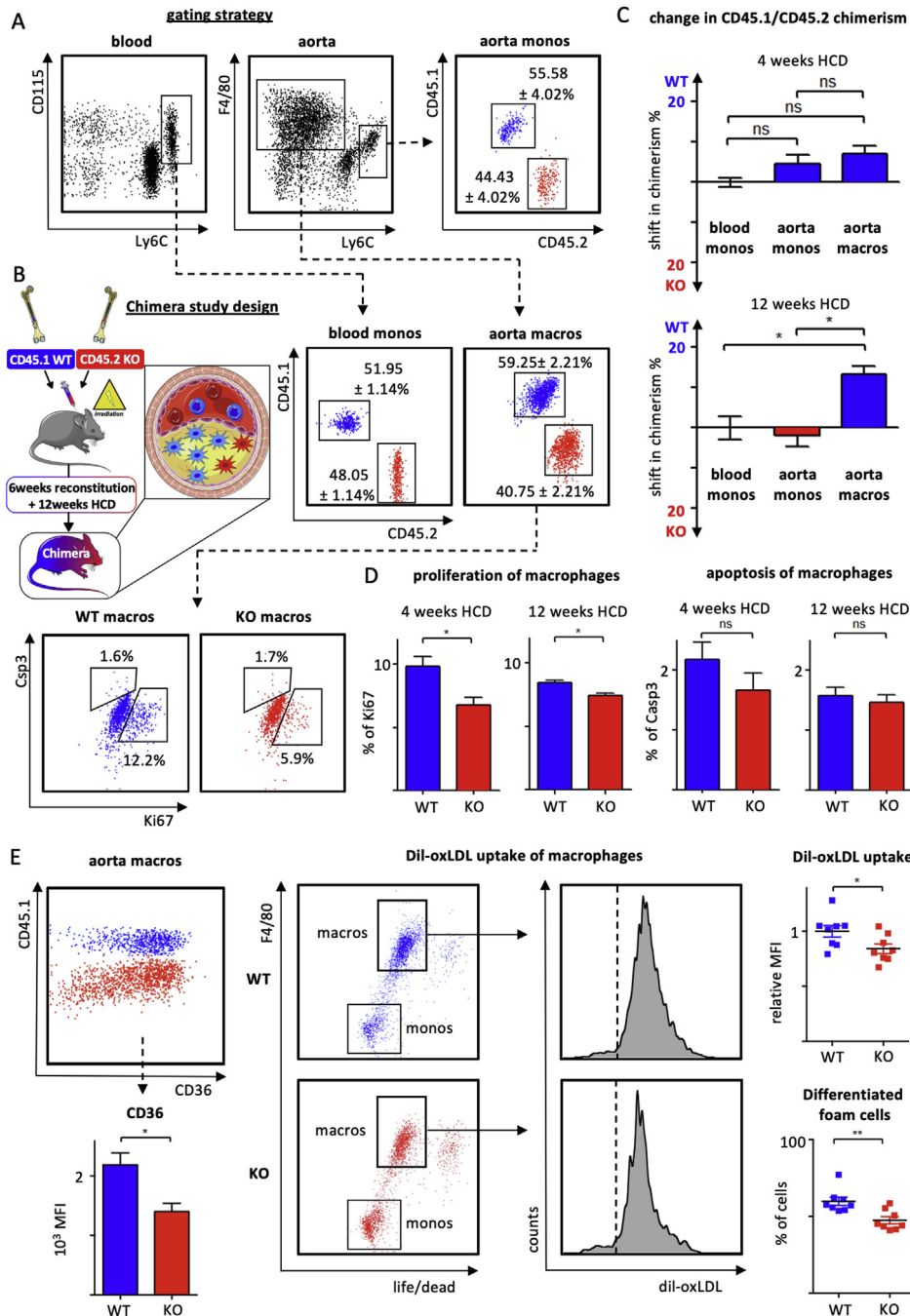


Figure 4: (A, B) Lethally irradiated *ApoE*^{-/-} mice were reconstituted with a mixture of *ApoE*^{-/-} CD45.1⁺ bone marrow cells (WT) and CD45.2⁺ *ApoE*^{-/-} *Lysm*^{Cre/+} *Irf5*^{fl/fl} bone marrow cells (KO) to create mixed chimeric mice. CD45.1 and CD45.2 chimerism was analyzed in monocytes and macrophages in the blood and aortic tissue cell suspension in mixed chimeras fed a high cholesterol diet for 4 weeks. Results are presented as mean \pm SEM, $n = 4$ mixed chimeras. (C) Relative change in CD45.1 and CD45.2 chimerism (%) between monocytes in the blood and aorta, and macrophages in the aorta is presented following 4 and 12 weeks of HCD feeding. Results are presented as mean \pm SEM, $n = 4$ –5 mixed chimeras, * $p < 0.05$ denotes statistically significant differences between cell populations, Kruskal–Wallis and Dunn’s multiple comparisons test. (D) Quantification of proliferation (Ki67) and apoptosis (Casp3) among aortic macrophages in mixed chimeras following 4 and 12 weeks of HCD. Results are presented as mean \pm SEM, $n = 4$ –5 mixed chimeras, * $p < 0.05$ denotes statistically significant intraindividual differences between CD45.1 (blue) and CD45.2 (red) macrophages, Mann–Whitney. (E) Quantification of CD36 surface expression on aortic macrophages in mixed chimeras following 12 weeks of HCD based on mean fluorescent intensities (MFI) as illustrated in the representative dot plot. CD45.1⁺ *Irf5*^{+/+} macrophages are shown in blue and CD45.2⁺ *Irf5*^{-/-} macrophages are shown in red. Results are presented as mean \pm SEM, $n = 4$ mixed chimeras, * $p < 0.05$ denotes statistically significant intraindividual differences between CD45.1 (blue) and CD45.2 (red) macrophages, Mann–Whitney. (F) Monocytes isolated from WT and KO mice were cultured with M-CSF for 16 h to induce macrophage differentiation, subsequently stimulated with DiI-labeled oxLDL for 4 h generating macrophage foam cells. Quantification of the fraction of differentiated F4/80^{high} foam cells and oxLDL uptake by flow cytometry (representative dot plots and histogram with dashed line representing unstimulated control). Results are presented as mean \pm SEM, $n = 8$ per group. * $p < 0.05$ denotes statistically significant differences between WT and KO, t-test. DiI-oxLDL = diI-labeled oxidized low density lipoprotein. HCD = high-cholesterol diet.

To study the functional relevance of *Irf5* expression in macrophages for the development of atherosclerosis, we generated a selective *Irf5* knockout (KO) in monocytes and macrophages of *Apoe*^{-/-} mice (Figure 2A).

3.2. *Irf5*-dependent macrophage polarization *in vitro*

First, macrophages were generated from bone marrow cells isolated from *Apoe*^{-/-} *Lysm*^{Cre/+} *Irf5*^{fl/fl} (KO) and *Apoe*^{-/-} *Irf5*^{fl/fl} (WT) mice, studying, *in vitro*, how the loss of *Irf5* under M1 and M2 polarizing conditions affected the expression of genes linked to key macrophage functions in the context of atherosclerosis: inflammation, efferocytosis and lipid transport (Figure 2B). Stimulation of BMDM with LPS and IFN γ -induced expression of M1-associated genes *Tnfa*, *Il12*, matrix metalloproteinase (*Mmp*) 2 and CC chemokine ligand (*Ccl*) 2, and suppressed gene expression of scavenger receptor *CD36* and cholesterol exporter ATP-binding cassette transporter (*Abca*) 1. *Irf5* deficiency blunted the increase in inflammatory M1 marker expression and suppressed *CD36* expression in polarized BMDM (Figure 2B). *Irf5*-deficient BMDM doubled the expression of *Mertk* when stimulated with LPS and IFN γ compared to *Irf5*^{+/+} BMDM. M2 polarization, by stimulating BMDM with IL-4 and IL-13, induced Arginase (*Arg*)1 expression, which remained unaffected by *Irf5* deficiency. However, mature *Irf5*^{-/-} BMDM already expressed elevated *Arg1* and *Abca1* levels without stimulation (M0) compared to *Irf5*^{+/+} BMDM. In summary, *Irf5* promoted inflammatory gene expression in macrophages *in vitro*. Next, we tested the effect of myeloid cell-specific IRF5 deficiency on atherogenesis *in vivo*.

3.3. Myeloid cell-specific *Irf5* deficiency promotes a stable plaque phenotype

Following 12 weeks of HCD, body weights, plasma cholesterol levels and leukocyte counts in blood, spleen and bone marrow (Figure 3 A, B and Supplemental Fig. 2) of myeloid cell-specific *Irf5*^{-/-} mice (*Apoe*^{-/-} *Lysm*^{Cre/+} *Irf5*^{fl/fl}; KO) did not differ from those in *Irf5*^{+/+} mice (*Apoe*^{-/-} *Irf5*^{fl/fl}; WT). Atherosclerotic lesion size and area at the aortic root level and aortic arch were similar in both groups, but plaque composition was altered (Figure 3 C, D, and Supplemental Fig. 3). Lipid and macrophage contents and necrotic core size were significantly reduced, and collagen contents increased in atherosclerotic lesions of KO mice compared to WT controls (Figure 3C and Supplemental Fig. 3). Accordingly, gene expression profiles of atherosclerotic aortas from KO mice showed a relative increase in *Tgfb*, *Mertk*, and *Cd206*, while *Ccl5* and *Il12* expressions were significantly reduced, with other inflammatory markers pointing towards the same direction (Figure 3E). Taken together, myeloid cell-specific *Irf5* deficiency promoted a stable plaque phenotype.

3.4. Multifactorial attenuation of *Irf5*-deficient macrophage accumulation in the plaque

Next, we generated mixed bone-marrow chimeras by reconstituting lethally irradiated *Apoe*^{-/-} mice with a mixture of CD45.1 *Apoe*^{-/-} (WT) and CD45.2 *Apoe*^{-/-} myeloid cell-specific *Irf5*^{-/-} (KO) bone marrow cells (Figure 4A,B). In these mice, *Irf5*-deficient and competent monocytes compete directly for accumulation in atherosclerotic lesions, and allow for assessing the intrinsic impact of *Irf5* deficiency in monocytes and their progeny, macrophages, in the plaque. Chimerism of *Irf5* WT and KO cells was determined by flow cytometric staining for CD45.1 and CD45.2 in the blood and aortic tissue cell suspensions (Figure 4A) as previously described [3,6]. In the blood of reconstituted *Apoe*^{-/-} mice fed a HCD for 4 weeks, 48.05 \pm 1.14% of circulating Ly6C^{high} monocytes were CD45.2⁺ and thus derived from the *Irf5* KO

bone marrow, while *Irf5* WT bone marrow gave rise to CD45.1⁺ Ly6C^{high} monocytes (51.95 \pm 1.14%). Interestingly, CD45.1/CD45.2 chimerism among Ly6C^{high} monocytes in the atherosclerotic aorta resembled the chimerism determined in the blood, indicating that *Irf5* KO monocytes were as likely as *Irf5* WT monocytes to infiltrate atherosclerotic lesions (Figure 4A,C). At 4 weeks of HCD, chimerism among aortic macrophages had already shifted slightly, yet not significantly, towards the CD45.1 WT population (+7.15 \pm 1.95%). With further plaque progression, following 12 weeks of HCD, the CD45.1⁺ *Irf5* WT macrophage population had outcompeted the CD45.2⁺ *Irf5* KO population significantly by 13.24 \pm 2.08%, while monocyte chimerism in the aorta still resembled CD45.1/CD45.2 chimerism in the blood (Figure 4C). These data suggest that *Irf5* deficiency impaired macrophage accumulation in the plaque, *in situ*, independent of monocyte recruitment as plaque development progressed. When determining local macrophage proliferation and apoptosis by flow cytometric staining for intracellular Ki67 and active Caspase 3, the frequency of proliferating macrophages was reduced in IRF5-deficient (CD45.2⁺) compared to *Irf5*-expressing cells (CD45.1⁺), whereas apoptosis remained unaffected (Figure 4D). Similarly, cell surface expression levels of *CD36* were quantified by flow cytometry measuring mean fluorescent intensity in *Irf5*-deficient (CD45.2⁺) and *Irf5*-expressing (CD45.1⁺) aortic macrophages. Expression of the lipid uptake receptor *CD36* was relatively reduced in *Irf5*^{-/-} macrophages (Figure 4E). To determine whether *Irf5* expression might influence monocyte to macrophage differentiation in the atherosclerotic plaque environment, we sorted Ly6C^{high} monocytes from peripheral blood and spleens of *Irf5* WT and KO mice and differentiated them into macrophage foam cells, *in vitro*, in the presence of oxidized (ox)LDL. Both the fraction of F4/80^{high} macrophages and the uptake of Dil-labelled oxLDL were reduced in *IRF5*-deficient cells (Figure 4F). In summary, *Irf5* deficiency within macrophages limited their accumulation in progressing plaques by hampering local macrophage differentiation, foam cell formation and proliferation.

4. DISCUSSION

Our study shows that *Irf5* expression is highly prevalent in, but not limited to, macrophages in atherosclerotic lesions in mice and men. Moreover, single-cell RNA sequencing documents that *Irf5* expression is not limited to one particular subcluster of macrophages in atherosclerotic aortas in *Apoe*^{-/-} mice and humans, although in human plaques, resident-like macrophages express lower levels of *IRF5* compared to both foamy and inflammatory subsets. A previous study, using immunofluorescent co-staining, showed that IRF5 protein expression associated with CD68 and CD11c but not alpha-smooth muscle actin (α SMA) in aortic root lesion of *Apoe*^{-/-} mice [36]. CD11c has been referred to as a M1 marker in atherosclerotic plaques [36,37], and our single-cell analysis confirms that CD11c expression is enriched in inflammatory and foamy macrophage clusters compared to M2/resident-like macrophages (Supplemental Fig. 1B). Having said this, *Irf5* expression does not correlate with CD11c expression in lesional macrophages according to our scRNA seq analysis (Supplemental Fig. 1C, E). The lack of co-localization of IRF5 expression and α SMA in atherosclerotic lesions, shown by Seneviratne et al., does not preclude that IRF5 can function in vascular smooth muscle cells (VSMC) in atherosclerotic lesions. VSMC that infiltrate the intima lose α SMA expression when transdifferentiating to macrophage-like cells [38], and VSMC in the media impact lesion formation by cell death, being replaced with extracellular matrix, and by increasing LDL deposition in the plaque [39,40]. Fibroblasts, mostly located in the

adventitia, are sources of inflammatory cytokines and growth factors [41,42], as are B-cells, which also serve as antigen-presenting cells secreting antibodies [43,44]. Our single-cell analysis reveals that IRF5 is expressed in these atheroma-associated cell types besides monocytes and macrophages, albeit at lower levels. To study the impact of IRF5 expression on atherogenesis selectively in monocytes and macrophages, we generated *Apoe*^{-/-} *Lysm*^{Cre/+} *Irf5*^{fl/fl} mice. First, we confirmed that bone marrow-derived macrophages in these mice expressed lower levels of inflammatory genes under M1 polarizing conditions. When fed an HCD to accelerate the formation of atherosclerotic lesions, these plaques featured an altered phenotype with reduced macrophage and lipid contents and increased collagen depositions. These phenotypic changes in female mice resembled those described by Seneviratne and colleagues, who studied systemic IRF5-deficient *Apoe*^{-/-} male mice on a chow diet [36]. As lesions progressed, the authors did not observe differences in lesion size at the aortic root level but detected smaller necrotic core areas. Because we fed *Apoe*^{-/-} mice a HCD, atherosclerotic lesions were more advanced and two to three times larger in our study. Moreover, in our study, the overall macrophage content was significantly reduced in plaques of myeloid cell-specific *Irf5*-deficient *Apoe*^{-/-} mice in contrast to the study by Seneviratne. Reduced CCL5 production in atherosclerotic aortas and attenuated monocyte to macrophage foam cell differentiation, in situ proliferation and oxLDL uptake likely contributed to the phenotype we present. Expression of *Cd36*, an oxLDL uptake mediating scavenger receptor, was reduced in M0- and M1-polarized BMDM in the absence of *Irf5*, and cholesterol exporter *Abca1* expression was increased, providing a mechanistic explanation for decreased foam cell formation and lipid deposition in the atherosclerotic plaques of myeloid cell-specific *Irf5*-KO mice. Notably, lipid uptake stimulates macrophage proliferation in the plaque, and CD36 cell surface expression was relatively reduced in *Irf5*^{-/-} aortic macrophages compared to *Irf5*^{+/+} macrophages in our chimeras [3,6]. Whether, in addition, IRF5 can regulate the transcription of cell cycle genes in macrophages, directly, as reported in B cells [45], is unknown. Seneviratne et al. reported that *Irf5* deficiency did not impact foam cell formation in GM-CSF-cultured BMDM following incubation with acetylated (ac)LDL. Of note, acLDL is mainly taken up via macrophage scavenger receptor 1 (*Msr1*), but not CD36, we reported recently [3]. *Msr1* expression was not significantly suppressed in *Irf5* deficient BMDM in our experiments, which may explain the discrepancies in the foam cell assay outcomes between the studies. *Mertk* expression was elevated in *Irf5*-deficient M1-polarized BMDM and in atherosclerotic aortas of myeloid cell-specific *Irf5*-deficient mice. *Mertk* is an essential efferocytosis-mediating receptor on macrophages, a process minimizing necrotic core formation in atherosclerotic lesions which become more fibrotic, as we show. Increased aortic *Tgfb1* expression in KO mice further supported collagen deposition, resulting in a stabilized plaque phenotype. Improved efferocytosis capacity was also postulated by Seneviratne et al. as the key mechanism for the favorable plaque phenotype observed in male *Apoe*^{-/-} *Irf5*^{-/-} mice on chow diet. Increased *Tgfb1* expression in visceral adipose tissue was reported in myeloid cell-specific *Irf5*^{-/-} mice consuming a high-fat diet [20].

Our results contrast with another study investigating the role of *Irf5* deficiency in lupus-associated atherosclerosis in *Apoe*^{-/-} mice carrying a gld point mutation in the gene encoding Fas ligand, which results in spontaneous autoimmune disease [46]. Although *Irf5* deficiency ameliorated lupus disease severity, atherosclerotic plaque formation exacerbated significantly. Contrasting with our study and the one by Seneviratne et al., *Irf5* deficiency augmented serum

cholesterol levels in the *Apoe*-deficient lupus mouse model. Notably, in these mice, both *Irf5*-deficient bone marrow-derived and non-bone marrow-derived cells contributed to the phenotype, confirming that IRF5 can also function in cells other than macrophages in the context of atherosclerosis.

This is why generating *Apoe*^{-/-} *Lysm*^{Cre/+} *Irf5*^{fl/fl} mice was essential to investigate the role of IRF5 selectively in monocytes and macrophages in the context of atherosclerosis. Our study provides a rationale for exploiting modulation of macrophage polarization, therapeutically, by showing that altering macrophage phenotypes can change plaque phenotypes.

ACKNOWLEDGMENTS

This work was supported by the German Research Foundation to I.H. (HI1573/2 and Collaborative Research Center SFB1425 grant 422681845) and to A.E. (grant 413517907, IMM-PACT program for Clinician Scientists, Department of Medicine II, Medical Center – University of Freiburg and Faculty of Medicine, University of Freiburg). J.L. was supported by the Otto-Hess-Scholarship from the German Cardiac Society.

CONFLICT OF INTEREST

None declared

APPENDIX A. SUPPLEMENTARY DATA

Supplementary data to this article can be found online at <https://doi.org/10.1016/j.molmet.2021.101250>.

REFERENCES

- [1] Al-Mallah, M.H., Sakr, S., Al-Qunaibet, A., 2018. Cardiorespiratory fitness and cardiovascular disease prevention: an update. *Current Atherosclerosis Reports* 20(1):1. <https://doi.org/10.1007/s11883-018-0711-4>.
- [2] Schaftenaar, F., Frodermann, V., Kuiper, J., Lutgens, E., 2016. Atherosclerosis: the interplay between lipids and immune cells. *Current Opinion in Lipidology* 27(3):209–215. <https://doi.org/10.1097/MOL.0000000000000302>.
- [3] Härdtner, C., Kornemann, J., Krebs, K., Ehlert, C.A., Jander, A., Zou, J., et al., 2020. Inhibition of macrophage proliferation dominates plaque regression in response to cholesterol lowering. *Basic Research in Cardiology* 115(6):78. <https://doi.org/10.1007/s00395-020-00838-4>.
- [4] Lindau, A., Härdtner, C., Hergeth, S.P., Blanz, K.D., Dufner, B., Hoppe, N., et al., 2016. Atheroprotection through SYK inhibition fails in established disease when local macrophage proliferation dominates lesion progression. *Basic Research in Cardiology* 111. <https://doi.org/10.1007/s00395-016-0535-8>.
- [5] Willemsen, L., de Winther, M.P., 2020. Macrophage subsets in atherosclerosis as defined by single-cell technologies. *The Journal of Pathology* 250(5):705–714. <https://doi.org/10.1002/path.5392>.
- [6] Robbins, C.S., Hilgendorf, I., Weber, G.F., Theurl, I., Iwamoto, Y., Figueiredo, J.-L., et al., 2013. Local proliferation dominates lesional macrophage accumulation in atherosclerosis. *Nature Medicine* 19(9):1166–1172. <https://doi.org/10.1038/nm.3258>.
- [7] Barrett, T.J., 2020. Macrophages in atherosclerosis regression. *Arteriosclerosis, Thrombosis, and Vascular Biology* 40(1):20–33. <https://doi.org/10.1161/ATVBAHA.119.312802>.
- [8] Alma, Zernecke, Holger, Winkels, Clément, Cochain, Williams Jesse, W., Dennis, Wolf, Oliver, Soehnlein, et al., 2020. Meta-analysis of leukocyte diversity in atherosclerotic mouse aortas. *Circulation Research* 127(3):402–426. <https://doi.org/10.1161/CIRCRESAHA.120.316903>.

- [9] Lin, J.-D., Nishi, H., Poles, J., Niu, X., Mccauley, C., Rahman, K., et al., 2019. Single-cell analysis of fate-mapped macrophages reveals heterogeneity, including stem-like properties, during atherosclerosis progression and regression. *JCI Insight* 4(4). <https://doi.org/10.1172/jci.insight.124574>.
- [10] Chinetti-Gbaguidi, G., Colin, S., Staels, B., 2015. Macrophage subsets in atherosclerosis. *Nature Reviews Cardiology* 12(1):10–17. <https://doi.org/10.1038/nrcardio.2014.173>.
- [11] Cardilo-Reis, L., Gruber, S., Schreier, S.M., Drechsler, M., Papac-Milicevic, N., Weber, C., et al., 2012. Interleukin-13 protects from atherosclerosis and modulates plaque composition by skewing the macrophage phenotype. *EMBO Molecular Medicine* 4(10):1072–1086. <https://doi.org/10.1002/emmm.201201374>.
- [12] Jefferies, C.A., 2019. Regulating IRFs in IFN driven disease. *Frontiers in Immunology* 10:325. <https://doi.org/10.3389/fimmu.2019.00325>.
- [13] Ren, J., Chen, X., Chen, Z.J., 2014. IKK β is an IRF5 kinase that instigates inflammation. *Proceedings of the National Academy of Sciences of the United States of America* 111(49):17438–17443. <https://doi.org/10.1073/pnas.1418516111>.
- [14] Lopez-Pelaez, M., Lamont, D.J., Pegg, M., Shpiro, N., Gray, N.S., Cohen, P., 2014. Protein kinase IKK β -catalyzed phosphorylation of IRF5 at Ser462 induces its dimerization and nuclear translocation in myeloid cells. *Proceedings of the National Academy of Sciences of the United States of America* 111(49):17432–17437. <https://doi.org/10.1073/pnas.1418399111>.
- [15] Krausgruber, T., Blazek, K., Smallie, T., Alzabin, S., Lockstone, H., Sahgal, N., et al., 2011. IRF5 promotes inflammatory macrophage polarization and TH1-TH17 responses. *Nature Immunology* 12(3):231–238. <https://doi.org/10.1038/ni.1990>.
- [16] Lazear, H.M., Lancaster, A., Wilkins, C., Suthar, M.S., Huang, A., Vick, S.C., et al., 2013. IRF-3, IRF-5, and IRF-7 coordinately regulate the type I IFN response in myeloid dendritic cells downstream of MAVS signaling. *PLoS Pathogens* 9(1):e1003118. <https://doi.org/10.1371/journal.ppat.1003118>.
- [17] Mai, L.T., Smans, M., Silva-Barrios, S., Fabié, A., Stäger, S., 2020. IRF-5 expression in myeloid cells is required for splenomegaly in L. Donovanii infected mice. *Frontiers in Immunology* 10. <https://doi.org/10.3389/fimmu.2019.03071>.
- [18] Duffau, P., Menn-Josephy, H., Cuda, C.M., Dominguez, S., Aprahamian, T.R., Watkins, A.A., et al., 2015. Interferon regulatory factor 5 promotes inflammatory arthritis. *Arthritis & Rheumatology (Hoboken, N.J.)* 67(12):3146–3157. <https://doi.org/10.1002/art.39321>.
- [19] Weihrauch, D., Krolikowski, J.G., Jones, D.W., Zaman, T., Bamkole, O., Struve, J., et al., 2016. An IRF5 decoy peptide reduces myocardial inflammation and fibrosis and improves endothelial cell function in tight-skin mice. *PLoS One* 11(4). <https://doi.org/10.1371/journal.pone.0151999>.
- [20] Dalmas, E., Toubal, A., Alzaid, F., Blazek, K., Eames, H.L., Lebozec, K., et al., 2015. Irf5 deficiency in macrophages promotes beneficial adipose tissue expansion and insulin sensitivity during obesity. *Nature Medicine* 21(6):610–618. <https://doi.org/10.1038/nm.3829>.
- [21] Hedl, M., Yan, J., Abraham, C., 2016. IRF5 and IRF5 disease-risk variants increase glycolysis and human M1 polarization by regulating proximal signaling and Akt2 activation. *Cell Reports* 16(9):2442–2455. <https://doi.org/10.1016/j.celrep.2016.07.060>.
- [22] Caplan, I.F., Maguire-Zeiss, K.A., 2018. Toll-like receptor 2 signaling and current approaches for therapeutic modulation in synucleinopathies. *Frontiers in Pharmacology* 9. <https://doi.org/10.3389/fphar.2018.00417>.
- [23] Ban, T., Sato, G.R., Tamura, T., 2018. Regulation and role of the transcription factor IRF5 in innate immune responses and systemic lupus erythematosus. *International Immunology* 30(11):529–536. <https://doi.org/10.1093/intimm/dxy032>.
- [24] Negishi, H., Ohba, Y., Yanai, H., Takaoka, A., Honma, K., Yui, K., et al., 2005. Negative regulation of Toll-like-receptor signaling by IRF-4. *Proceedings of the National Academy of Sciences of the United States of America* 102(44):15989–15994. <https://doi.org/10.1073/pnas.0508327102>.
- [25] Lawrence, T., Natoli, G., 2011. Transcriptional regulation of macrophage polarization: enabling diversity with identity. *Nature Reviews Immunology* 11(11):750–761. <https://doi.org/10.1038/nri3088>.
- [26] Günthner, R., Anders, H.-J., 2013. Interferon-regulatory factors determine macrophage phenotype polarization. *Mediators of Inflammation*, 731023. <https://doi.org/10.1155/2013/731023>.
- [27] Weiss, M., Blazek, K., Byrne, A.J., Perocheau, D.P., Udalova, I.A., 2013. IRF5 is a specific marker of inflammatory macrophages in vivo. *Mediators of Inflammation*, 245804. <https://doi.org/10.1155/2013/245804>.
- [28] Singh, G.B., Zhang, Y., Boini, K.M., Koka, S., 2019. High mobility group box 1 mediates TMAO-induced endothelial dysfunction. *International Journal of Molecular Sciences* 20(14):3570. <https://doi.org/10.3390/ijms20143570>.
- [29] Habich, C., Baumgart, K., Kolb, H., Burkart, V., 2002. The receptor for heat shock protein 60 on macrophages is saturable, specific, and distinct from receptors for other heat shock proteins. *The Journal of Immunology* 168(2):569–576. <https://doi.org/10.4049/jimmunol.168.2.569>.
- [30] Curtiss, L.K., Tobias, P.S., 2009. Emerging role of Toll-like receptors in atherosclerosis. *Journal of Lipid Research* 50:S340–S345. <https://doi.org/10.1194/jlr.R800056-JLR200>.
- [31] Wirka, R.C., Wagh, D., Paik, D.T., Pjanic, M., Nguyen, T., Miller, C.L., et al., 2019. Atheroprotective roles of smooth muscle cell phenotypic modulation and the TCF21 disease gene as revealed by single-cell analysis. *Nature Medicine* 25(8):1280–1289. <https://doi.org/10.1038/s41591-019-0512-5>.
- [32] Winkels, H., Ehinger, E., Vassallo, M., Buscher, K., Dinh, H.Q., Kobiyama, K., et al., 2018. Atlas of the immune cell repertoire in mouse atherosclerosis defined by single-cell RNA-sequencing and mass cytometry. *Circulation Research* 122(12):1675–1688. <https://doi.org/10.1161/CIRCRESAHA.117.312513>.
- [33] Stuart, T., Butler, A., Hoffman, P., Hafemeister, C., Papalexi, E., Mauck, W.M., et al., 2018. Comprehensive integration of single cell data. *BioRxiv*, 460147. <https://doi.org/10.1101/460147>.
- [34] Butler, A., Hoffman, P., Smibert, P., Papalexi, E., Satija, R., 2018. Integrating single-cell transcriptomic data across different conditions, technologies, and species. *Nature Biotechnology* 36(5):411–420. <https://doi.org/10.1038/nbt.4096>.
- [35] Stuart, T., Butler, A., Hoffman, P., Hafemeister, C., Papalexi, E., Mauck, W.M., et al., 2019. Comprehensive integration of single-cell data. *Cell* 177(7):1888–1902. <https://doi.org/10.1016/j.cell.2019.05.031> e21.
- [36] Seneviratne, A.N., Edsfeldt, A., Cole, J.E., Kassiteridi, C., Swart, M., Park, I., et al., 2017. Interferon regulatory factor 5 controls necrotic core formation in atherosclerotic lesions by impairing efferocytosis. *Circulation* 136(12):1140–1154. <https://doi.org/10.1161/CIRCULATIONAHA.117.027844>.
- [37] Ono, Y., Nagai, M., Yoshino, O., Koga, K., Nawaz, A., Hatta, H., et al., 2018. CD11c⁺ M1-like macrophages (M Φ s) but not CD206⁺ M2-like M Φ are involved in folliculogenesis in mice ovary. *Scientific Reports* 8. <https://doi.org/10.1038/s41598-018-25837-3>.
- [38] Basatemur, G.L., Jørgensen, H.F., Clarke, M.C.H., Bennett, M.R., Mallat, Z., 2019. Vascular smooth muscle cells in atherosclerosis. *Nature Reviews Cardiology* 16(12):727–744. <https://doi.org/10.1038/s41569-019-0227-9>.
- [39] Hamczyk, M.R., Villa-Bellosta, R., Gonzalo, P., Andrés-Manzano, M.J., Nogales, P., Bentzon, J.F., et al., 2018. Vascular smooth muscle-specific progerin expression accelerates atherosclerosis and death in a mouse model of hutchinson-gilford progeria syndrome. *Circulation* 138(3):266–282. <https://doi.org/10.1161/CIRCULATIONAHA.117.030856>.
- [40] Hamczyk, M.R., Andrés, V., 2018. Accelerated atherosclerosis in HGPS. *Aging* 10(10):2555–2556. <https://doi.org/10.18632/aging.101608>.
- [41] Tillie, R.J.H.A., van Kuijk, K., Sluimer, J.C., 2020. Fibroblasts in atherosclerosis: heterogeneous and plastic participants. *Current Opinion in Lipidology* 31(5):273–278. <https://doi.org/10.1097/MOL.0000000000000700>.

- [42] Xu, F., Ji, J., Li, L., Chen, R., Hu, W., 2007. Activation of adventitial fibroblasts contributes to the early development of atherosclerosis: a novel hypothesis that complements the “Response-to-Injury Hypothesis” and the “Inflammation Hypothesis”. *Medical Hypotheses* 69(4):908–912. <https://doi.org/10.1016/j.mehy.2007.01.062>.
- [43] Sage, A.P., Tsiantoulas, D., Binder, C.J., Mallat, Z., 2019. The role of B cells in atherosclerosis. *Nature Reviews Cardiology* 16(3):180–196. <https://doi.org/10.1038/s41569-018-0106-9>.
- [44] Hilgendorf, I., Theurl, I., Gerhardt, L.M.S., Robbins, C.S., Weber, G.F., Gonen, A., et al., 2014. Innate response activator B cells aggravate atherosclerosis by stimulating T helper-1 adaptive immunity. *Circulation* 129(16):1677–1687. <https://doi.org/10.1161/CIRCULATIONAHA.113.006381>.
- [45] De, S., Zhang, B., Shih, T., Singh, S., Winkler, A., Donnelly, R., et al., 2017. B cell-intrinsic role for IRF5 in TLR9/BCR-induced human B cell activation, proliferation, and plasmablast differentiation. *Frontiers in Immunology* 8:1938. <https://doi.org/10.3389/fimmu.2017.01938>.
- [46] Watkins, A.A., Yasuda, K., Wilson, G.E., Aprahamian, T., Xie, Y., Maganto-Garcia, E., et al., 2015. IRF5 deficiency ameliorates lupus but promotes atherosclerosis and metabolic dysfunction in a mouse model of lupus-associated atherosclerosis. *The Journal of Immunology* 194(4):1467–1479. <https://doi.org/10.4049/jimmunol.1402807>. Baltimore, Md.